Journal of Inflammation Research

Dovepress
Taylor & Francis Group

Open Access Full Text Article

ORIGINAL RESEARCH

P300-Targeted Acetylome Reveals a Role for HMGB1 Translocation in Central Cardiac Sympathetic Activation Post Myocardial Infarction

Jie Yin[1,2,*], Fuhong Liu[2,3,*], Huitang Xia[4], Suhua Yan[2], Ye Wang[2], Xinran Li[2], Yugen Shi[2], Yu Wang[2], Yanyan Jing[5], Yan Li[3,6], Hesheng Hu[2]

[1]Department of Cardiology, Shandong Provincial Hospital affiliated with Shandong First Medical University, Jinan, Shandong, People's Republic of China; [2]Department of Cardiology, the First Affiliated Hospital of Shandong First Medical University & Shandong Provincial Qianfoshan Hospital, Jinan, Shandong, People's Republic of China; [3]Medical Research Center, the First Affiliated Hospital of Shandong First Medical University & Shandong Provincial Qianfoshan Hospital, Jinan, Shandong, People's Republic of China; [4]Department of Plastic Surgery, the First Affiliated Hospital of Shandong First Medical University and Shandong Provincial Qianfoshan Hospital, Jinan, Shandong, People's Republic of China; [5]Department of Cardiology, Yantai Yuhuangding Hospital, Yantai, Shandong, People's Republic of China; [6]Shandong Province University Clinical Immunology Translational Medicine Laboratory, The First Affffliated Hospital of Shandong First Medical University and Shandong Provincial Qianfoshan Hospital, Jinan, Shandong, People's Republic of China

*These authors contributed equally to this work

Correspondence: Hesheng Hu; Yan Li, Email huhesheng@sfdmu.edu.cn; yli@email.sdfmu.edu.cn

Background: Microglia/macrophage-dominated neuroinflammation in the hypothalamic paraventricular nucleus (PVN) critically mediates sympathetic overactivation, with the underlying mechanism remained elusive. Given that protein acetylation serves as a pivotal epigenetic modifier of inflammatory responses to immune-microenvironmental changes, we aimed to explore the role of acetyltransferase p300 in the pathophysiological process of sympathetic activation post-myocardial infarction (MI).

Methods and Results: Rats MI model was established by ligating LAD artery. During early stage, p300 was increased in the PVN and mainly localized on microglia. Microinjection of short-hairpin RNA (shRNA) targeting p300 into the PVN effectively knocked down p300 expression, resulting in reduced peripheral sympathetic nerve activity and decreased cardiac norepinephrine levels. Programmed electrical stimulation post-MI revealed that p300 knockdown decreased ventricular arrhythmia (VA) susceptibility. p300-regulated acetylome was analyzed using shotgun proteomics in human HCM3 cells, and 135 target acetylated proteins were identified. Bioinformatic analysis and coimmunoprecipitation assays revealed that p300 interacted with and acetylated high-mobility group protein B1 (HMGB1). P300 facilitated the cytoplasmic translocation of HMGB in microglia in vivo, thereby contributing to cardiac sympathetic activation. Protein docking analysis and brain slice patch-clamp recordings revealed the potential interaction between HMGB1 and excitatory glutamate receptor N-methyl-D-aspartate receptor (NMDAR) levels. Rescue experiments employing patch-clamp electrophysiology with a recepor-specific inhibitor confirmed direct mediation of HMGB1 in neuronal activation through NMDAR-dependent mechanisms.

Conclusion: Microglial p300-mediated translocation of HMGB1 in the PVN may be a fundamental epigenetic mechanism in NMDAR-mediated central sympathetic activation post-MI, suggesting targeting p300 signaling modulation in the PVN as a potential antiarrhythmic therapy.

Keywords: acetylation, p300, myocardial infarction, paraventricular nucleus, sympathetic activation

Introduction

Cardiovascular diseases (CVD) are major global health burden worldwide,[1,2] whereas myocardial infarction (MI) is the most severe form of CVD that accounts for the leading cause of death.[2] Fatal ventricular arrhythmias (VAs) remain the primary causes of sudden cardiac death (SCD) among patients with acute MI.[3] Sympathetic hyperactivation is one of the major causes of ventricular arrhythmogenesis.[4–6] Investigation into possible interventions and the underlying

Received: 22 February 2025
Accepted: 10 September 2025
Published: 4 November 2025

Graphical Abstract

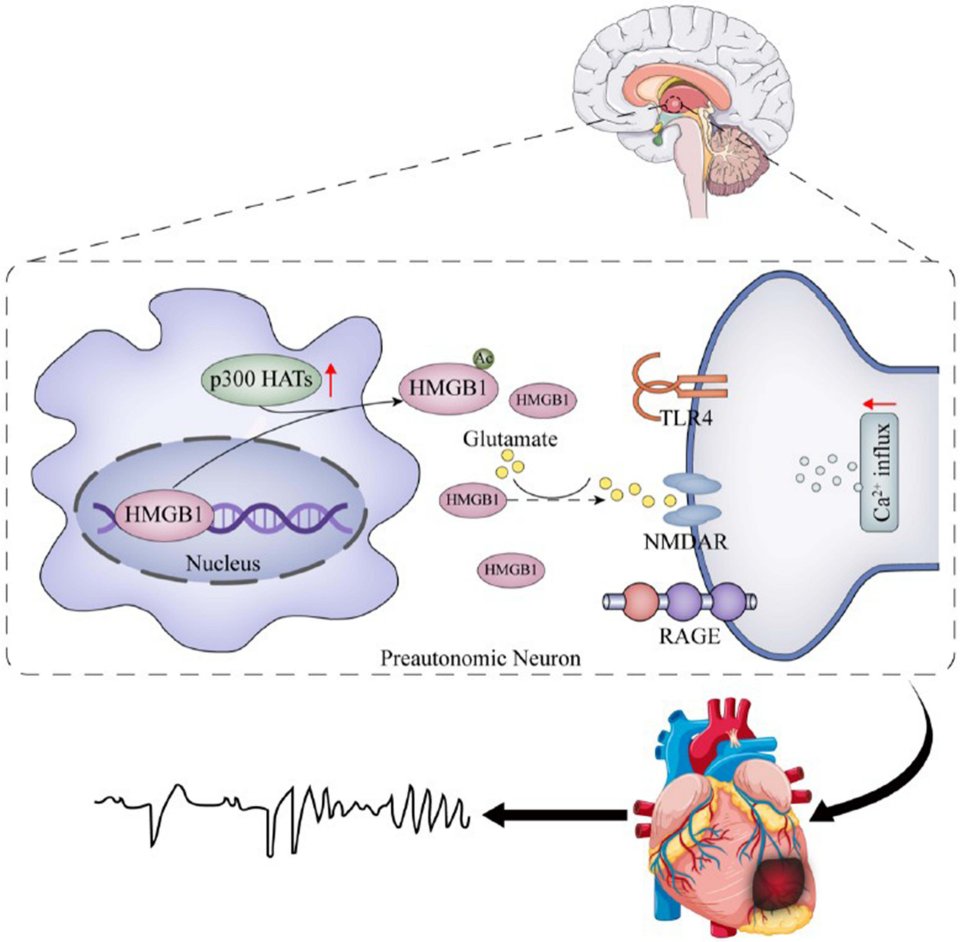

mechanisms of VA post-MI has mainly focused on the cardiac sympathetic nerves, however, the brain-cardiac axes in the pathogenesis of sympathetic overactivation remain poorly understood. Accumulating evidence has suggested that central paraventricular nucleus (PVN) within the hypothalamus is the most important regulator of autonomic nervous tone and involves in cardiovascular homeostasis regulation. Recently, we found that microglia-mediated inflammation within the PVN exacerbated VAs by increasing sympathetic tone and ventricular arrhythmia susceptibility,[7] yet the precise mechanism remains unclear.

Protein post-translational modifications, including methylation, phosphorylation, and acetylation, are emerging as key mediators of cardiovascular pathogenesis following changes in immuno-microenvironment.[8] Acetylation, the most common and conserved PTM, is important for protein function modification, including trans localization, binding partners interaction, conformation, catalytic activity, and stability. Lysine acetyltransferases (KAT), containing of MYST, GNAT and p300/CBP families, are responsible for histone and non-histone protein acetylation. It is evidenced that cardiovascular diseases change the acetylation status, participating various process, including cardiac remodeling and arrhythmia.[9] Here, we explored the role of the acetyltransferases in the pathogenesis of sympathetic hyperactivity post-MI. In the present study, we found that among the acetyltransferases, p300 acetyltransferase (KAT3B) (HGNC: 3373) was specifically upregulated in PVN tissue post-MI. P300 is a large scaffold protein shuttling between the nucleus and cytoplasm following its N-terminal nuclear localization signals (NLS). Adeno-associated virus (AAV) vector carried

short hairpin RNA (shRNA) was utilized for p300 silencing within PVN, to determine the role of p300 signaling in sympathoexcitation. Label-free proteomic technique combining enrichment identified for acetylated peptides downstream p300. We then conducted a series of bioinformatic analysis to classified p300 substrates into different pathways and identified the downstream target HMBG1. The current study will unveil the pathological process of central-cardiac sympathetic activation and provide new strategies for VAs therapy post-MI.

Methods

AMI Model

Male Sprague-Dawley rats (~225 g; Beijing HFK Bioscience, China) were utilized in this study. All experimental procedures were performed in complied with the protocols approved by the Laboratory Animal Ethics Committee of the First Affiliated Hospital of Shandong First Medical University (QFSYYPZ2019022201). Open-chest surgery was conducted following 7 days adaption. Briefly, rats were anaesthetized by intraperitoneal injection of 3% pentobarbital sodium (30 mg/kg) and ventilated via tracheal intubations connected to a rodent ventilator as previously described.[7] Following the heart exposure via incising along the left fourth intercostal space, a 6–0 polypropylene suture was carefully passed beneath the left anterior descending (LAD) coronary artery at the standard ligation site, approximately 2–3 mm distal to the junction between the conus arteriosus and left atrial appendage.[10] The Sham group underwent all the surgery protocol without ligation on the heart. Then, the rats were allowed to recover on a heated pad to maintain a body temperature of 37°C after surgery. Finally, then they were returned to their individual cages. The rats were closely monitored at the first 24–72 h after surgery. Successful infarction was defined by observing the immediate ST elevation in electrocardiogram, regional wall motion abnormality and cyanosis were common criteria for infarction confirmation.[11] The survival rate was 88% 3 h following the coronary ligation.

Experimental Design

Protocol 1

Thirty of the 37 surviving rats were assigned to five groups (0, 1, 3, 5, and 7 days; n = 6/group). The expression of acetyltransferases was detected using real time-PCR), whereas the temporal expression pattern of p300 was detected by Western blotting.

Protocol 2

A total of 106 rats were randomly assigned to the following four groups to ensure an approximately equal number of survivors in each: Group A (sham + shCtrl; n = 20), Group B (sham + shp300; n = 20), Group C (MI + shCtrl; n = 21), and Group D (MI + shp300; n = 22). The virus was administered bilaterally to the PVN using a stereotaxic apparatus (RWD Life Science, China) following the three-dimensional coordinates (lateral: 0.4 mm, posterior: 1.8 mm, and 7.9 mm deep to the bregma).[7] P300 knockdown was conducted using recombinant virus AAV1/2 vectors carrying p300 small hairpin RNAs (shp300) or scrambled shRNA (shCtrl) over-expressed under U6 promoter with co-expression of GFP as reporter under CMV promoter (Shanghai Genechem Co., China). To guarantee effective p300 silencing, three targeting sequences were selected: CCGGCACTGTGCATCTTCTCGACAATTCAAGAGATTGTCGAGAAGATGCACAGTGTTTTTG, CCGGAACAGTGGCACGAAGATATTATCAAGAGATAATATCTTCGTGCCACTGTTTTTTTG, and CCGGGAGCACGACTTACCAGATGAATTCAAGAGATTCATCTGGTAAGTCGTGCTCTTTTTG. Ultimately, the last one was selected. About 50 nl of either shp300 or a scrambled shCtrl (titer: 1.5×10^{12} genomic particles/mL) were separately administrated into PVN using microinjector.[7] The microinjector was removed 15 min after injection. Four weeks later, the rats received MI surgery. On day 7 post-MI, the rats subject to Telazol intraperitoneally injection and isoflurane inhalation following the electrophysiological study.

RNSA

Renal sympathetic nerve activity (RSNA) serves as an indicator for peripheral sympathetic tone.[12] Seven days after the MI surgery, the left renal nerve was dissected and carefully disassociated with surrounding tissue. Then, the left renal nerve was cut distally to eliminate the effect of afferent activity. The nerve was hooked using a pair of bipolar silver-wire

recordings. A four-channel AC/DC differential amplifier (AD Instruments, Sydney, Australia) with a band-pass filter ranging from 100 to 3000 Hz was applied for signals amplification (time constant: 10ms; sampling frequency: 10 kHz).[7] Background noise measurement was conducted at the end of each experiment.

In vivo Electrophysiological Experiments

Ventricular Arrhythmias (VAs) Susceptibility was conducted with Mapping lab, and ECG recording electrodes were placed on the left ear and right ventricle. Electrical stimulation (MappingLab, VCS-3001, 30 mV) was applied to the left ventricle of the heart. The stimulation protocol was applied by TTL generator software. In brief, eight S1 beats with a cycle length of 120 ms followed by one to three extrastimuli in shorter coupling intervals were applied. The programmed stimulation, VAs inducibility quotient qualified by VA scores were detailed described in published study.[13]

Tissue Collection

Following the electrophysiological study, the entire brain was then excised following decapitation. Brain and heart tissues were prepared for further analysis: i) The PVN was dissected from the brain tissue and transferred to −80°C storage immediately for subsequent molecular biology experiments. (2) For immunohistochemical study, the whole brain was fixed in 10% formalin and alternatively underwent paraffin section or continuing immersed in 15%, 30% sucrose for gradient dehydration until sinking completely to the bottom, and then embedded in Tissue-Tek® OCT compound and frozen on ice for 5 min before stored at –80°C for subsequent immunofluorescence analysis. (3) Additionally, the heart and peripheral blood were harvested. The middle section of hearts containing the infarcted myocardium was stored in 4% formalin and embedded in paraffin for Masson's staining.

Histological Test

Following standard protocols, the infarct size was evaluated by Masson's staining of heart cross section (Nanjing Jiancheng Technology, China).[14] Planimetry was utilized to analyze digitized images, and the infarcted size was presented as the percentage of fibrosis area/total left ventricle area.

Immunohistochemistry analysis was applied to assess central sympathetic activation via the Fos family. A mouse anti-c-Fos antibody (1:1000, Abcam, ab208942) was applied. The slides were incubated with goat anti-mouse (HRP) (1:200, Servicebio, G1214) and the DAB chromogenic kit (AIDACX Biotechnology, PNSJH-08). They were then counterstained with hematoxylin.

Frozen tissue double/multiplex immunofluorescence staining was performed according to the protocol of a staining kit (Absin Bioscience Inc., abs50012). Briefly, following antigen retrieval with a rapid antigen retrieval solution and antigen blocking with QuickBlock™ Blocking Buffer (Beyotime, Nanjing, China), primary antibodies mouse anti-p300 (1:500, Abcam, ab275379), rabbit anti-Iba1 (1:500, Abcam, ab178846), rabbit anti-HMGB1 (1:250, Abcam, ab79823) and/or rabbit anti-NMDAR1 (1:200, ABclonal, A7677) was used. After incubated at room temperature for 2 h or 4°C overnight, the sections were washed and incubated with the secondary antibody in the kit for 40 min, then fluorescence amplification solution was used for 15 min each. Furthermore, DAPI solution (Abcam, ab104139) was used to identify the nuclei. Finally, fluorescence images were viewed and captured with a confocal microscope (Nikon, Japan). Ten random microscopic fields were selected and then analyzed using ImageJ software (version 1.38).

RT-PCR

Real time-PCR was performed to measure target mRNA levels.[8] Briefly, total RNA was obtained by Trizol reagent and reverse transcribed into cDNA with cDNA Synthesis kit (Yeasen, China). RT-qPCR assay was performed using a SYBR qPCR Master Mix (Takara, Japan) in CFX96 Real-Time System. For quantification, GAPDH was utilized as a reference for sample normalization. Both the target gene and GAPDH were repeated in triplicate for each sample. A $2^{-\Delta\Delta CT}$ method was applied for relative quantification in comparison between groups. The list of PCR primers sequences is presented in Supplementary Table S1, which were designed by Primer-Blast tool in NCBI. We further confirmed primer specificity in by confirming that the amplification curve is a single exponential curve, and the dissolution curve is a single peak in the process of qPCR.

Western Blot

Cytoplasmic and nuclear proteins were separately extracted using the Nucleocytoplasmic Separation Kit (Beyotime, China; P0027). The following primary antibodies were utilized, with their respective dilutions: anti-HMGB1 rabbit pAb (1:10,000, Abcam, ab79823), anti-p300 rabbit pAb (1:1000, Abcam, ab275379), and acetylated lysine antibody (1:1000, Cell Signaling, #9441). β-tubulin and histone 3 served as internal references. The Ac-HMGB1 levels were referenced to total HMGB1 protein. Band intensity was quantified using scanning densitometry.

Enzyme-Linked Immunosorbent Assay (ELISA)

Myocardial tissue was minced by low temperature freezing grinder and suspended in perchloric acid (0.4 N) with reduced glutathione (5 mmol/L; pH 7.4). Then, the supernatants were collected following immediate centrifugation. Then, a commercial ELISA kit (USCN Life Science, LMC681Ra) was applied to measure cardiac norepinephrine concentration.

Cell Preparation

HCM3 and HEK293 cells were purchased from ATCC and cultured following the company's instructions. In brief, RPMI-1640 medium and 10% FBS was used. For p300 siRNA transfection, the HMC3 cells were seeded in 6-well plates and nurtured to up to 30%–50% confluency. ShRNA directed against p300 (5'-GAGCACGACTTACCAGATGAA-3') or scramble control (5'-TTCTCCGAACGTGTCACGT-3') were transiently transfected into HMC3 cells, and INTERFERin®(Polyplus) transfection reagent was applied according to the instructed protocol. For plasmid transfection, the HEK293 cells (1×10^5 cells per well) were plated on 3.5 cm dish and cultivated to 70% confluence. Polyethylenimine (PEI, 25 kDa, Polysciences) 3 μg was added with 2 μg of plasmids into each well. Cellular analysis was conducted 48–72 h following siRNA treatment.

Mass Spectrometry Analyses

Acetylated Label-Free Method

Protein samples were extracted and quantified using SDT Lysis Buffer and BCA Protein Assay Kit. Total proteins were reduced with DTT, and iodoacetamide was used to block the reduced cysteine residues. Subsequently, trypsin (Promega) was used for digestion and peptide mixture collection, followed by enrichment of Kac using the Acetyl-Lysine Motif Kit (Cell Signaling Technology, 13416S). Samples were separated using a Nano Elute (Bruker, Germany) system with a nanoliter flow rate connected to a Q Exactive HF-X mass spectrometer (Thermo Fisher Scientific) equipped with a CaptiveSpray ion source for mass spectrometry identification. The mass spectrometry data were searched using Maxquant software from the Uniprot_HomoSapiens_20386_20180905 database. A global false discovery rate cutoff of 0.01 was set for peptide and protein identification. Lysine acetylation sites with a fold change >2 or <0.5 and an uncorrected *P*-value (*t*-test) <0.05 were considered significantly different.

Bioinformatics Analysis

Gene Ontology (GO) Enrichment

All protein sequences were aligned with the NCBI database, retaining sequences that ranked in the top 10 with an E-value ≤1e3. Subsequently, Blast2GO was used to complete the GO term annotation. InterProScan was utilized to conduct motif-based searches in the European Bioinformatics Institute database and augment functional information on the motif in proteins to improve annotation. Fisher's exact test was used to compare the differentially expressed proteins and total proteins correlated using GO terms. Finally, the bubble plot in the enrichment plot package was used to show the GO enrichment results. The procedure above complied with the principles drafted in the Declaration of Helsinki.

Screening Differentially Expressed Proteins

Based on the protein expression profile, we conducted a cluster analysis of differentially expressed proteins using the heatmap package. The protein expression data were normalized for cluster analysis. The results are presented as a heat map.

Expression Plasmids and shRNA

The acetylation of NLS lysine is essential for protein cytoplasm translocation and release in immune cells.[15] There are two NLSs identified, one located in the A box (aa 28–44) and the other in the B box (aa 179–185).[16] To express these in HEK293 cells, we cloned complementary DNAs encoding wild-type HMGB1, HMGB1 A box, HMGB1 B box, point mutations of lysine K28/29/30/43/44 to arginine (R), and p300 into a plasmid cloning DNA vector.

Coimmunoprecipitation

HEK293 cells were harvested, washed with freezing phosphate buffered saline, and lysed on ice for 30 min with a lysis buffer (150 mM NaCl, 0.5% NaD OC, 50 mM Tris-HCl (pH 7.5), 1% NP40, 1 mM Na_2EDTA, and 10% glycerol) containing protein inhibitors (cocktail, 1 mM Na_3VO_4, 10 mM NaF, and 1 mM PMSF). The supernatants were immunoprecipitated after centrifugation of the cell lysates at 4°C. This involves incubating with antibodies while rotating for 1 h at 4°C, followed by incubating with protein A/G-agarose beads for another 1 h, and subsequently washed the bead for 4 times with lysis buffer. Then, Western blotting and immunoprecipitation were conducted as described previously.[17]

Patch Clamp Study

Paraventricular Nucleus Slice Recordings

Viable brain slices were obtained from animals that were transcardial perfused with CSF (glycerol based artificial cerebrospinal fluid). The CSF contained 252 mM glycerol, 1.2 mM NaH_2PO_4, 1.2 mM MgCl, 1.6 mM KCL, 2.4 mM $CaCl_2$, 26 mM $NaHCO_3$, 11 mM glucoses. Removed the brain carefully and sliced the brain into 300 μm thickness which contained paraventricular nucleus (PVN) neurons marked by the third ventricle. Transfer the brain slices to a solution comprising: 110 mM N-methyl D-glucamine, 1.2 mM NaH_2PO_4, 2.5 mM KCl, 25 mM $NaHCO_3$, 110 mM HCl, 25 mM glucose, 10 mM $MgSO_4$, and 0.5 mM $CaCl_2$. Equilibrated the solution at 37°C for 15 minutes with 95% O_2 and 5% CO_2. Transfer the slices into a superfusion recording chamber with perfusion solution containing 125 mM NaCl, 2 mM $CaCl_2$, 3 mM KCl, 5 mM glucose, 26 mM $NaHCO_3$, and 5 mM HEPES. The perfusion solution was equilibrated with 5% CO_2 and 95% O_2 at 25°C. Equilibrate each slice in this perfusion solution for 30 minutes. Visualize the PVN Neurons with differential interference contrast optics and record the neurons with the prepared patch pipette. Patch pipettes, with the resistance of 5–7 MΩ, were filled with an intracellular solution (ICS) containing of 135 mM K-gluconic acid, 10 mM EGTA, 10 mM HEPES, 1 mM $MgCl_2$, and 1 mM $CaCl_2$. The PVN neurons were then patched and clamped in the voltage recordings mode with a holding potential of −70 mV using Axon 700B and pClamp 10.3 software (Axon Instruments). CNQX (50 mM) and APV (50 mM) were applied by the end of the experiment to block glutamatergic AMPA/kainate and NMDA receptors, respectively, which would confirm that the EPSCs were glutamatergic. The amplitudes and frequency spontaneous mEPSCs were analyzed to assess the differences of synaptic transmission in PVN fibers between groups.

In vitro Neuron Recordings

Disinfect the neonatal 24 h SD rats with the 75% alcohol spray. And soaked the rats in 75% alcohol for 3–5 min and then decapitated at the head/neck junction using the small surgical scissors. The paraventricular nucleus (PVN) was isolated following the previously described protocols.[18] Briefly, separated the PVN, and placed the PVN in HBSS (Invitrogen, NY) enriched with glucose and sectioned into small pieces for enzymatic digestion. Collagenase II (2 mg/mL, 15–25 min) was used to digest PVN tissues at 37°C. After digestion, collect the isolated single PVN neurons by centrifugation at 1000 rpm/5 min. These cells were then seeded on coverslips and cultured for 7–10 days with 2% B27 serum in a neurobasal medium (Gibco).

The patch recordings were applied on the PVN neurons. EPC10 patch-clamp amplifier was used in this experiment. Collected and analyzed the electrical signals using a Patchmaster system (HEKA Elektronik, Germany). Pull the recording pipettes of a resistance of 3–5 MΩ. The SF-77B fast perfusion (Warner) system was addressed to perfuse or deliver chemicals onto the cells with extracellular solution (ECS). The ECS consisted of: 130 mM NaCl, 2 mM $MgCl_2$, 2 mM $CaCl_2$, 5 mM KCl, 10 mM glucose, 10 mM HEPES, and 10 mM sucrose, pH = 7.4, and the osmolarity was 310. The pipettes solution consisted of: 115 mM Cs-$MeSO_3$, 5 mM NaCl, 10 mM CsCl, 10 mM HEPES, 20 mM TEA, 0.6 mM EGTA, 0.3 mM Na_3GTP, 4 mM Mg-ATP, and 10 QX-314 (pH = 7.2), and the osmolarity was 300. For NMDA receptor-

mediated miniature EPSCs (NMDA-mEPSCs), $MgCl_2$ was 0 and the ECS was supplemented with 10 μm CNQX, 50 μm picrotoxin, 1 μm strychnine, and 15 μm glycine. To record AMPA receptor-dependent miniature EPSCs (AMPA-mEPSCs), we supplemented the ECS with 2 mM $MgCl_2$, 1 μM TTX, 50 μM picrotoxin, and 50 μM APV.[19] The exogenous HMGB1 (40 nM) was added into the ECs when recording NMDA/AMPA-mEPSCs respectively. Hold the membrane potential at −70 mV unless otherwise specified. Filtered the recordings at 2 kHz and sampled at 5 kHz. Mini-analysis software was used to analyze the mEPSCs in this study.

Statistical Analysis

SPSS17.0 was used for statistical analysis. *t* test, analysis of variance (ANOVA) with post hoc tests were used to analyse the differences among groups. Quantitative results were shown as Mean ± SD. $p < 0.05$ was considered statistically different.

Results

P300 Was Especially Upregulated, Predominantly in Microglia in the PVN Following MI

We examined lysine acetyltransferase (KAT) enzymes alterations using a real-time PCR array at day 3 post-MI to elucidate the acetylation regulation mechanism which may affect central sympathetic activation, since VAs events increased within 3 days of AMI onset as previously reported.[20] Among the selected 33 KATs, only 22 were detected. P300 was the most significant upregulated acetyltransferase (Figure 1A). Western blot detection showed that p300 exhibited a slight upregulation after 1 day, was significantly overexpressed on day 3, and remained at a high level beyond day 7 (Figure 1B and C). Increased p300 immunoreactivity was noted within the PVN on AMI rats (Figure 1D and Figure S1). Interestingly, p300 was primarily co-stained with microglia marker Iba1 (Figure 1D–F). These data revealed the potential role of p300 in regulating microglia.

P300 Participated in the Pathogenesis of Sympathetic Overactivition Post-MI

To uncover the role of p300 in the pathogenesis of MI, we constructed a AAV1/2-U6-p300/scramble shRNA-CMV-GFP and microinjected it into the PVN following protocol 2 (Figure 2A). GFP expression was detected with microscopic to confirm the specific distribution of the administered virus in the PVN (Figure 2B). The efficacy of the p300 knockdown was verified through Western blotting (Figure 2C and D). Furthermore, the morphology changes were analyzed on day 7 post MI (Table 1). Masson staining ruled out those less than 30% of infarct size due to lack of clinical significance. Our data revealed a reduced infarcted area in the MI-shp300 group than those in the MI-shCtrl group ($P < 0.05$), coinciding with ameliorating cardiac dysfunction as indicated by the index of ejection fraction (Figure 2E–H).

Next, the central and peripheral sympathetic function was investigated. Immunohistochemical staining of Fos protein served as an indicator of central sympathetic activation. As a result, MI triggered widespread neuronal activation significantly throughout the PVN evidenced by upregulation of Fos protein level. In contrast, administration of p300 shRNA significantly down-regulated Fos expression (Figure 3A and D). RSNA levels represented peripheral sympathetic tone was then evaluated. As shown Figure 3B, the baseline RSNA post infarction was significantly higher than that underwent sham surgery ($P < 0.05$). Additionally, RSNA levels were significantly attenuated in the MI + shp300 group compared to those in the MI + shCtrl group ($P < 0.05$). Consequently, reduced ventricular arrhythmias vulnerability with p300 knockdown mirrored those of RSNA content (Figure 3C–F). The increasing levels of cardiac NE (Figure 3G) post-MI, which reflecting cardiac sympathoexcitation, was reversed by p300 shRNA administration.

Characterization of the p300-Dependent Acetylome

To identify the specific substrates downstream p300 acetylation, we performed an unbiased screen through MS-based proteomics. This involves comparing acetylated proteins in scramble RNA transfected cells with those in cells where p300 has been silenced. We utilized two stable HMC3 cell lines in which doxycycline was used to induce the expression of control shRNA (NC) or shRNA targeting p300 (KC). The efficiency of the p300 knockdown was verified using Western blot analysis. We identified 135 differential acetylated protein between control and p300 knockdown group. The

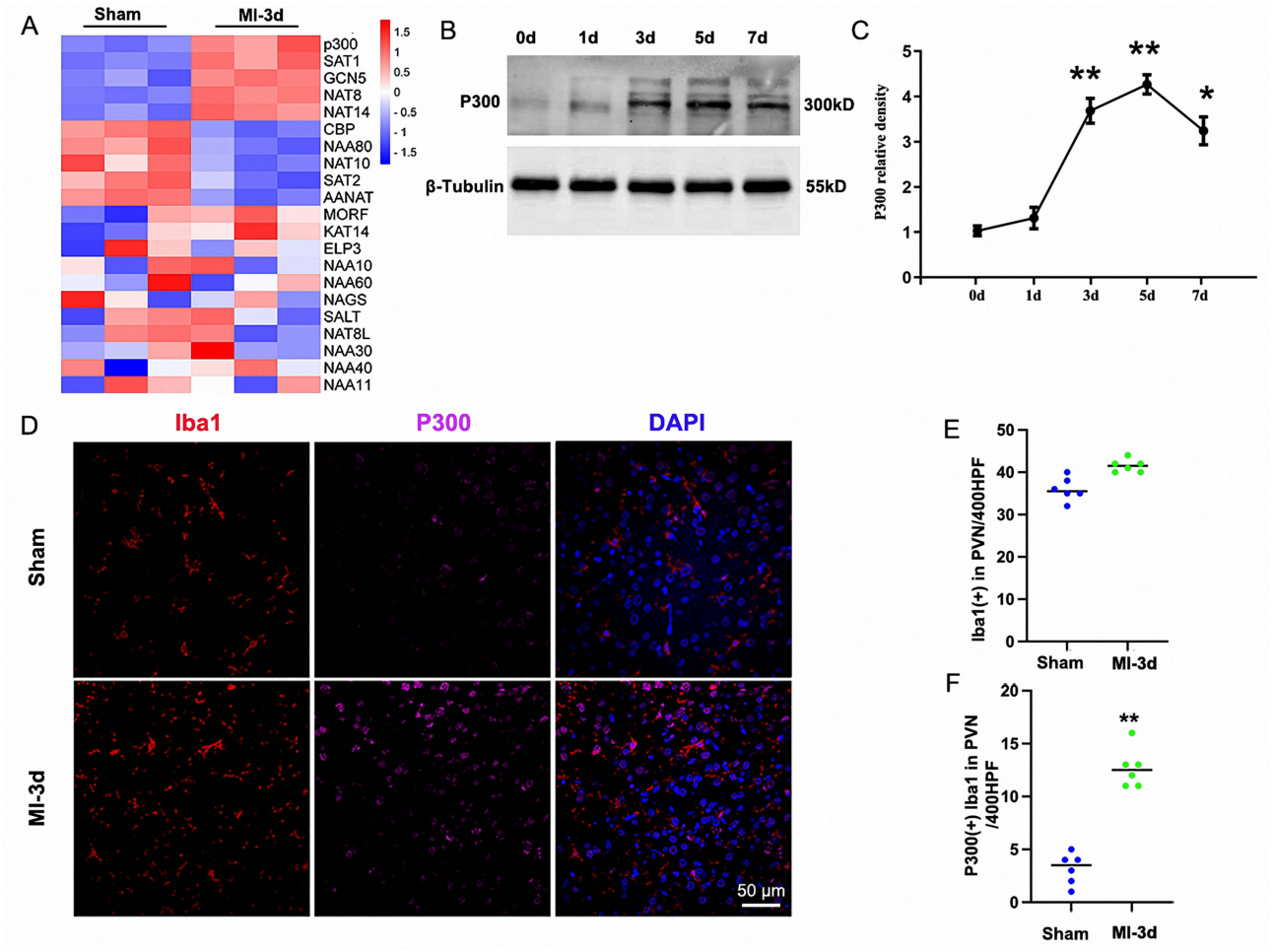

Figure 1 Expression profile of the p300 in PVN post-MI. (**A**) A summary heatmap of quantitative RT-PCR analysis of acetyltransferase. n = 3 per group. (**B** and **C**) Western blot showing the expression profiles of p300 (300 kD) in PVN at 0 hr, 1-, 3-, 5-, and 7-days post-MI. P300 was quantified relative to the β-tubulin (55 kD) levels. n = 4 per group and per time-point. (**D**) Double-immunostaining for Iba1 (green) and p300 (red) in the vehicle-MI group shows a limited distribution of p300 on Iba1 in the PVN. Bar = 30 μm. (**E** and **F**) Qualification of Iba1 positive and p300 positive Iba1 cells in PVN, respectively n = 6 per group. *T* test and two-way analysis of variance (ANOVA) were applied for two groups and four groups analysis respectively. Each column with a bar represents the mean ± standard deviation. **P* < 0.05 and ***P* < 0.01 vs 0 hr.
Abbreviations: MI, myocardial infarction; PVN, paraventricular nucleus, RT-PCR, reverse transcription polymerase chain reaction, HPF: high power field.

heatmap showing the top 12 differentially acetylated proteins (Figure 4A). GO enrichment analysis showed that p300 is involved in biological processes, mainly included cellular processes, cellular component organization, biological regulation or developmental processes, biogenesis, protein transport, response to stimulus, and immune system processes (Figure 4A and B). Examples of proteins acetylated by p300 enriching in the same biological processes according to GO term analysis were presented in Figure 4C and D. According to previous study, protein transport and release from microglia played an important role in microglia-neuron crosstalk.[21] Therefore, we hypothesized that p300-mediated protein transport serves as a bridge between microglia and neural activation. Then, we focused on the protein transport related genes. Among them, HMGB1 was most significant differential protein as indicated in heatmap in Figure 4A. HMGB1 has been demonstrated as the key bridge between microglia-neuron communication,[22] therefore, we tested whether HMGB1 is the downstream target for p300 mediated sympathoexcitation.

P300 Directly Induces Nucleus-Cytoplasm Translocation and Release of HMGB1 in Microglia Post-MI

The nucleocytoplasmic translocation of HMGB1 was markedly increased in the PVN among MI rats; in contrast, acetyltransferase p300 silencing significantly partially reversed MI-induced HMGB1 cytoplasmic translocation as

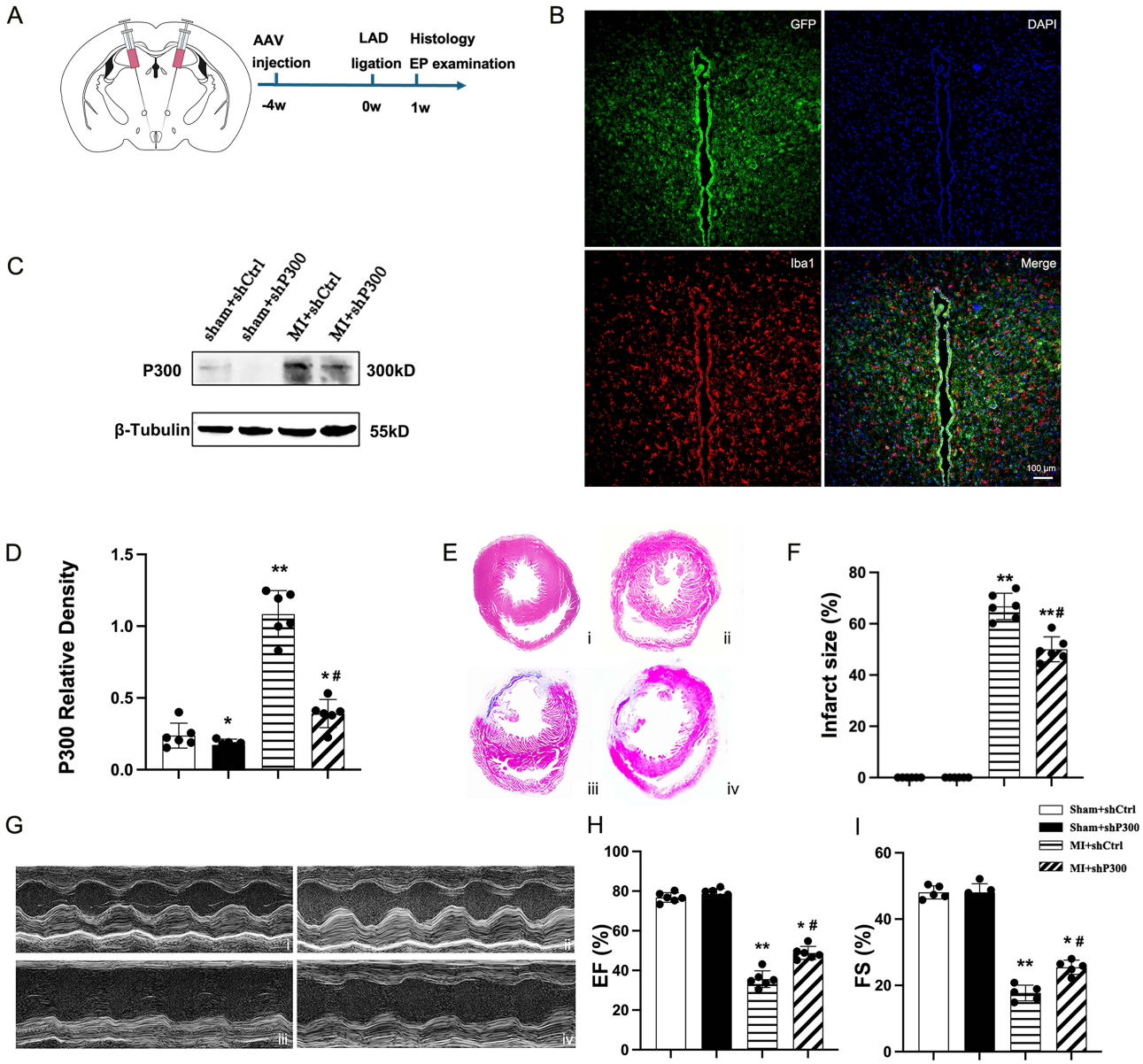

Figure 2 Targeted p300 knockdown in PVN. (**A**) Sketch map of targeting virus injection into PVN using stereotaxic apparatus. (**B**) Image confirming PVN targeted virus transfection into microglia. (**C**) Representative expression of p300 at 7 days post-MI as determined via Western blotting. (**D**) P300 expression was quantified relative to the β-tubulin (55 kD) levels. (**E**) Representative original color images of Masson's trichrome staining of the infarcted area: (i) sham group, (ii) sham + shCtrl, (iii) MI + shp300 and (iv) MI + shCtrl. (**F**) Infarction size calculation by Image J. (**G**) Representative images of cardiac function recorded by M-mode echocardiography. Ejection Fraction (EF) calculation (**H**) and fractional shortening (FS) calculation (**I**). n = 6 per group. Two-way ANOVA was applied for statistical analysis. Each column with a bar represents the mean ± SD. **P* < 0.05, ***P* < 0.01 vs sham + shCtrl group; # *P* < 0.05 vs MI + shCtrl group.
Abbreviations: MI, myocardial infarction; PVN, paraventricular nucleus.

showed in immunofluorescence staining (Figure 5A and D, E). Similar tendency in nucleocytoplasmic translocation and enhanced HMGB1 acetylation were found, as revealed through Western blot analysis (Figure 5B and C, F, G). Our finding further suggests that nonacetylation states correlate with nuclear retention, whereas p300-mediated acetylation promotes cytosolic trans localization as indicated by immunofluorescence and Western blot.

P300 Directly Interacts with HMGB1 with K43 the Key Acetylated Lysine Site

Full-length HMGB1 contains two NLSs located in the HMGB1-A box (aa 28–44) and HMGB1-B box (aa 179–185), which guide the protein translocate into the nucleus. These lysine residues are conserved in HMGB1 across species, from Drosophila to humans (Figure S2), suggesting their functional relevance. To figure out the specific region of HMGB1

https://doi.org/10.2147/JIR.S524375

Table 1 Cardiac Morphology at the End of the Study

Parameters	Sham Surgery		Ligation Surgery	
	shCtrl	shp300	shCtrl	shp300
No. of surviving rats	20	20	21	22
Survival rate, %	100	100	75	78.5
Body weight, g	386 ± 12	381± 10	356 ± 12	362± 8
Heart Rate, bpm	424 ± 15	430 ± 12	452 ± 16*	448 ± 12*
EF	85 ± 6	86 ± 8	40 ± 5*	49 ± 6*
Infarcted Size (%)			65.8 ± 4.5%	43.6 ± 5.2%*†

Notes: Values are mean ± SD. *$p < 0.05$ compared with respective sham group; †$p < 0.05$ compared with vehicle treated infarcted groups treated with shCtrl.

which undergoes acetylation by p300, we conducted co-transfection using truncation mutants Flag-tagged HMGB1 or wild-type HMGB1 plasmids with myc-tagged p300 into HEK293T cells. Subsequently, they were subjected to reciprocal coimmunoprecipitation (CO-IP) experiments, revealing that p300 acetylates HMGB1 with the A box (Figure 6A). Subsequently, we generated flag-tagged acetylation-mimicking non-acetylated (K28R, K29R, K30R, K43R, and K44R) mutants of HMGB1. CO-IP analysis revealed that the point mutation at lysine 43 to arginine significantly reduced the binding affinity between p300 and HMGB1 (Figure 6B). Following this, we examined the effects of p300 on HMGB1 translocation by immunofluorescence confocal imaging and found that HMGB1K43R mutants blocked HMGB1 cytoplasmic translocation and acetylation (Figure 6C–F). Eventually, ELISA analysis showed that K43R mutants consequently attenuating HMGB1 release level (Figure 6G).

Increased NMDAR Activity in Presympathetic Neurons Through the p300-HMGB1 Axis

Next, we sought to resolve whether p300 mediated HMGB1 traslocation participated in postsynaptic excitation. Enhanced glutamatergic input in PVN, especially the NMDAR activity, is a major source of the excitatory drive to sympathetic tone. Interestingly, despite of the functional variation of glutamate receptors, the protein level of NMDAR kept unchanged (Figure 7A–C). However, the amplitude and frequency of basal glutamatergic excitatory postsynaptic currents (mEPSCs) of PVN neurons was significantly greater in MI group than in sham group. Consistently, p300 knockdown significantly reversed the attenuated NMDAR-mEPSC (Figure 7D–G).

Given the above evidence highlighting the critical role of macrophage-derived HMGB1 in central sympathetic activation, we assumed that HMGB1 may influence excitatory glutamate receptors function directly. Consistently, immunofluorescence experiments revealed colocalization of HMGB1 and NMDARs in primary PVN neurons post-MI (Figure 8A). Molecular docking using Discovery Studio 2016 software to predict the potential binding affinity between HMGB1 and NMDAR subunits. As a result, a strong binding affinity between HMGB1 and GluN1 and GluN2B subunits were found (highest Zdock score: 22.1 and 20.9, respectively; Figure 8B). Patch-clamping study further revealed that HMGB1 significantly enhanced both the amplitude and current numbers of mEPSCs in PVN neurons without affecting the half-width of mEPSCs (Figure 8C and D). To define the precise role of NMDARs in HMGB1-induced firing hyperactivity, we applied intracellular dialysis with an NMDAR channel specific blocker MK-801 to block NMDARs. When neurons were pretreated with the MK-801, the substantial increase in EPSCs was significantly decreased. Furthermore, HMGB1 induced a marked increase in NMDA puff-elicited currents, but it did not affect AMPA-mEPSCs in PVN neurons (Figure 8E–G). This indicates a direct role for HMGB1 in NMDAR-mediated neuronal activation.

Discussion

The conception of brain-spleen and gut-brain axes had been raised and studied in detail;[23,24] however, the brain-cardiac axes remained poorly understood. The PVN plays a crucial role in regulating cardiovascular activity and sympathetic

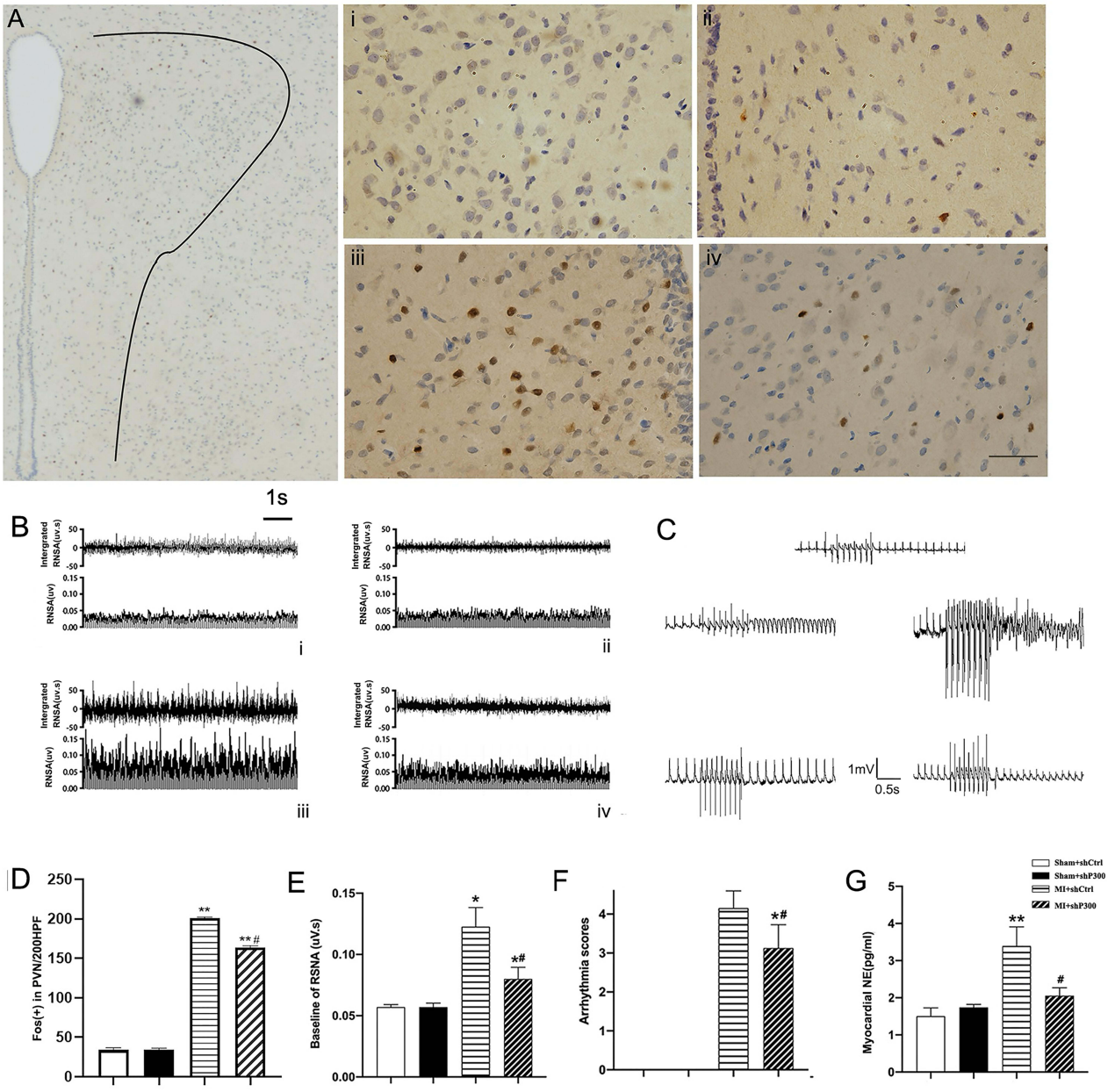

Figure 3 Effects of p300 on sympathetic nerve activity and programmed electrical stimulation at 7 days post-MI. (**A**) Representative immunohistochemical images of central sympathetic nerve activity marked using Fos family proteins, indicated by brown puncta. Nuclei (blue) were stained with hematoxylin: (i) sham + shCtrl, (ii) sham + shp300, (iii) MI + shCtrl, and (iv) MI + shp300 groups (magnification 200×). Bar = 50 μm. (**B**) Typical recordings from the left RSNA and integrated RSNA at 7 days post-MI in (i) sham + shCtrl, (ii) sham + shp300, (iii) MI + shCtrl, and (iv) MI + shp300 groups. Bar = 1s. (**C**) Typical inducible ventricular arrhythmias. (**D**) Quantitation of Fos-positive cells. (**E**) Quantification of baseline of RSNA. (**F**) Quantification of ventricular arrhythmia scores. (**F**) Comparisons of the arrhythmia scores across four groups. The vertical bar = 1mV, abscissa bar = 0.5s. (**G**) Myocardial NE levels detected by ELISA. n = 6 per group. Two-way ANOVA was applied for statistical analysis. Data are expressed as mean ± S.D. $^{**}P < 0.01$ and $^{*}P < 0.05$ vs the sham group. $\#P < 0.05$ vs the MI + shCtrl groups.

Abbreviations: MI, myocardial infarction; NE, norepinephrine; RSNA, renal sympathetic nerve activity; SD, standard deviation.

outflow, serving as an important interface between peripheral inflammation and the central nervous system mechanisms responsible for regulating cardiac sympathetic activity.[7] In the current study, we identified the role of acetylase p300 on central-cardiac sympathetic hyperactivity post-MI. Specifically, p300 mediated immuno-neuron communication via promoting microglia HMGB1 nuclear-cytoplasm translocation; then translocated HMGB1 further combined with preganglionic NMDAR and facilitates sympathetic activation. This information has the potential to improve the current

https://doi.org/10.2147/JIR.S524375

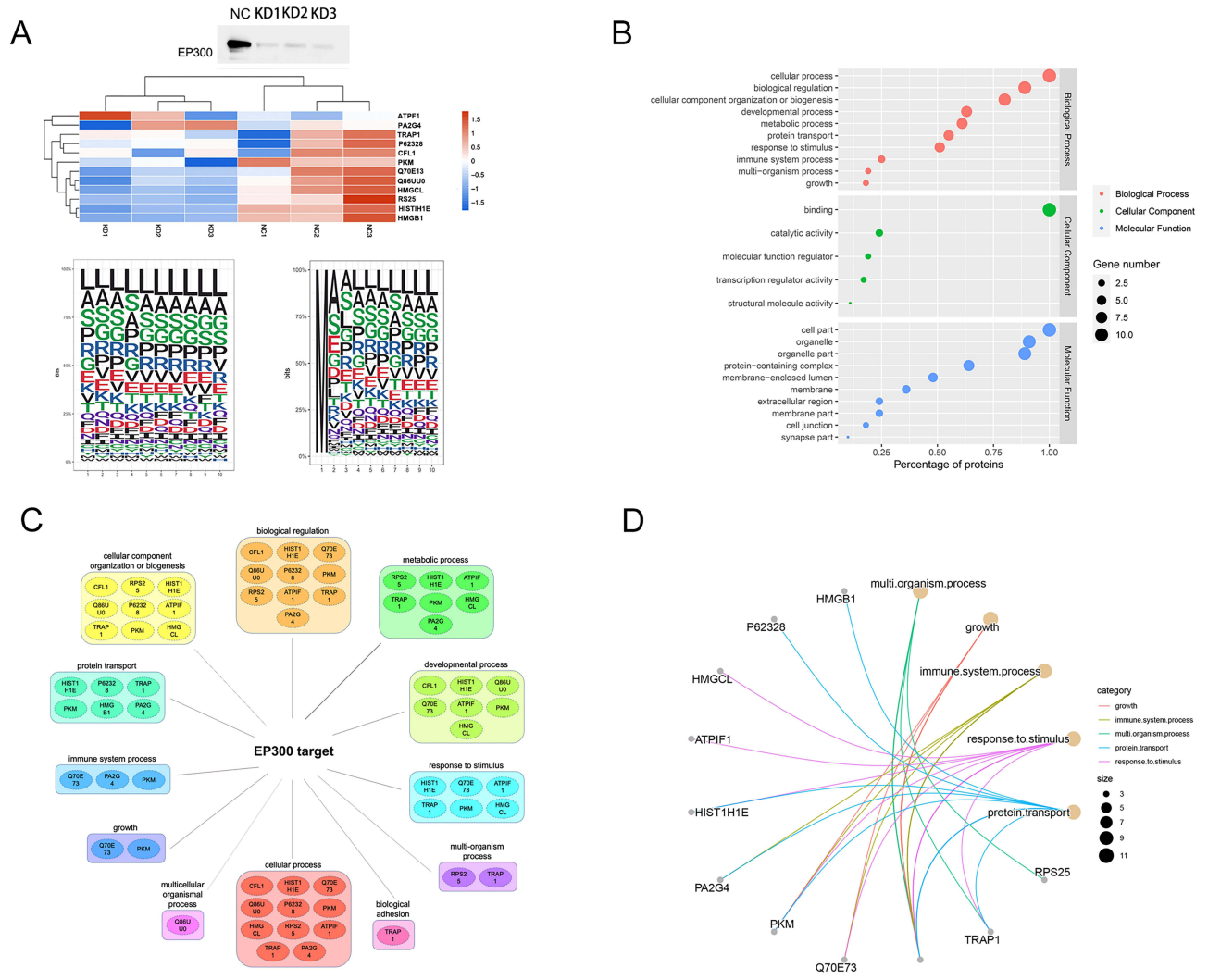

Figure 4 Identification of p300-dependent acetylome. (**A**) (upper panel); (lower panel) Ice logo shows analysis of the frequency of amino acids surrounding the acetylated lysines targeted by p300. Overall, we analyzed 159 distinct "Ks" derived from a list of 135 proteins, with 10 aa upstream (−10 on the x-axis) and 10 aa downstream (+10 on the x-axis). The overall height of the stack indicates the sequence conservation at that position, while the symbol height within the stack indicates the relative frequency of each amino acid at that position. (**B**) Go enrichment analysis of proteins acetylated by p300 in biological process, cellular component and molecular function. (**C**) Based on GO enrichment analysis, the cnetplot of proteins acetylated by p300 suggests HMGB1 is involved in the protein transport process. (**D**) Motif logo map depicting p300 binding protein in NC and KD groups.

Abbreviations: GO, gene ontology; HMGB1, high-mobility group protein B1.

knowledge and update education surrounding brain-cardiac axes in the pathogenesis of post-MI arrhythmia, as well as microglia-neuron crosstalk in sympathoexcitation.

Cardiac autonomic imbalance by overactivation of central sympathetic outflow in PVN connects tightly with arrhythmogenesis post-MI.[25,26] Inflammatory stress is acknowledged as the master regulator of numerous pathological processes that lead to sympathetic activation, with the underlying mechanism remained poorly understood.[27] Accumulating evidence indicates that, alongside genetic factors, epigenetic mechanisms transducing the effects of gene-microenvironment interactions contribute to inflammation-mediated pathophysiological processes following injury, such as MI and stroke.[28] We explored the epigenetic mechanisms underlying acetylation during central sympathetic nervous system activation.

KATs are well-known for targeting Lys sites on N-terminal tails of histone, whereas acetyltransferase p300, the most widely studied KAT, has long been shown to acetylate many Lys residues in non-histone proteins and modifies the stability, localization, and DNA-binding capability of the latter.[29,30] Specifically, p300 plays critical roles in regulating inflammation response by transporting of proteins involved in inflammation.[17] Accordingly, we observed a significant

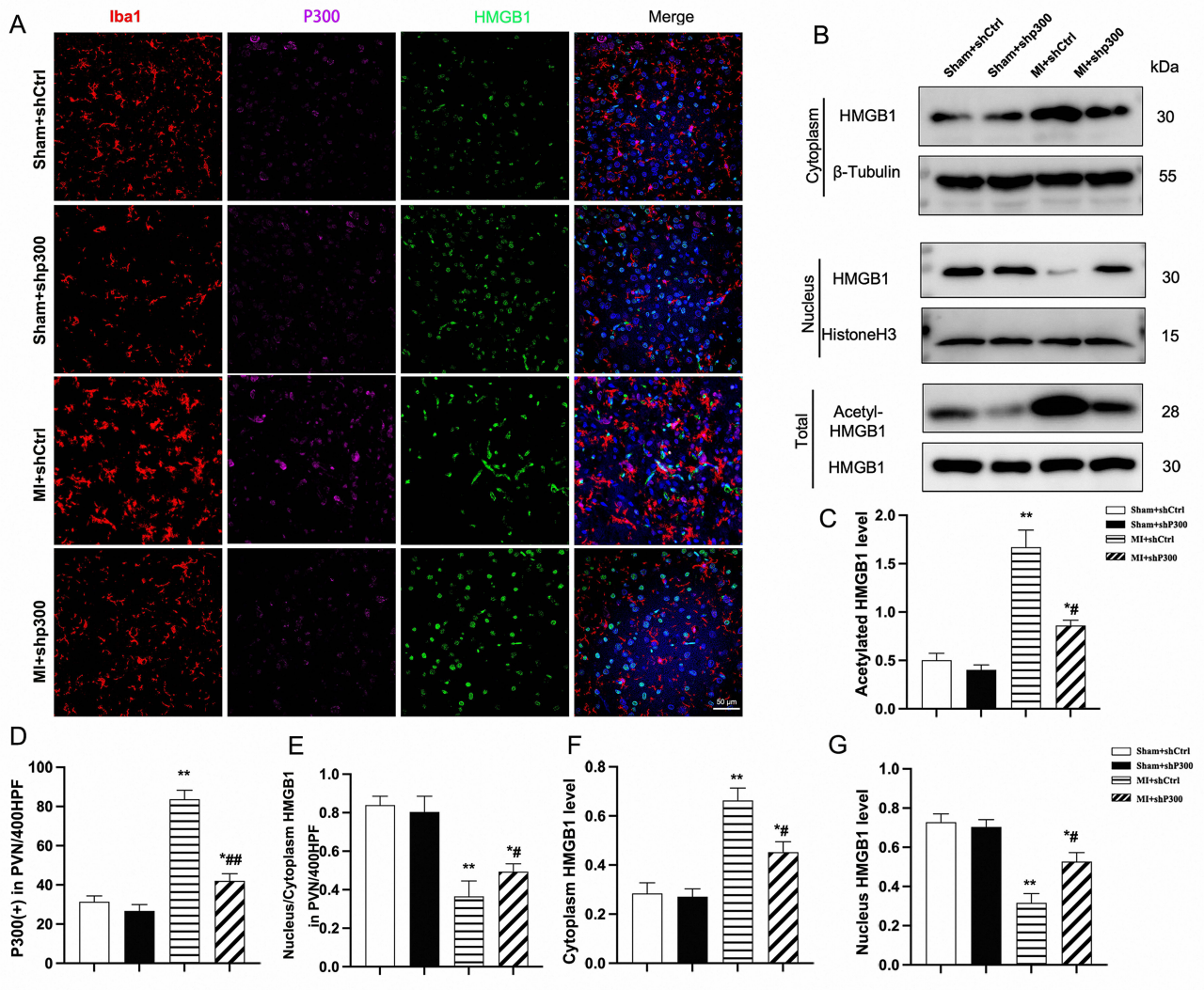

Figure 5 The effect of p300 shRNA intervention on HMGB1 levels, intracellular distribution, and acetylation in the PVN of MI rats. (**A**) Immunofluorescence costaining for HMGB1 (cyan) with Iba1 (green) and p300 (red) of PVN 7 days after MI. (**B**) Representative Western blot illustrating cytoplasm/nucleus/acetylation HMGB1 protein. (**C**) Qualification of acylation level of HMGB1. (**D** and **E**) Qualification of p300 positive cells and nucleus/cytoplasm HMGB1 percentage in PVN, respectively. (**F** and **G**) Qualification of cytoplasm and nucleus HMGB1 level, respectively. Bar = 30 μm. n = 6 per group. Two-way ANOVA was applied for statistical analysis. Values are expressed as the mean ± SD. *P < 0.05 and **P < 0.01 vs the sham group; # #P < 0.01, #P < 0.05 vs the MI + shCtrl groups.
Abbreviations: HMGB1, high-mobility group protein B1; MI, myocardial infarction; PVN, paraventricular nucleus; HPF: high power field.

increase in the expression of p300, specifically within the microglia of the PVN post-MI, as opposed to other acetyltransferases. Simultaneously, targeting delivery of p300 shRNA to PVN ameliorated sympathetic overactivation and ventricular arrhythmia. This supports the presence of a novel epigenetic mechanism underlying inflammation-related sympathetic activation. Next, we aimed to sought out the downstream target of p300 from HCM3 cell lines by label free acetylation omics mass spectrometry study. We found 135 differential acetylated protein involved in various biological process, such as biogenesis, cellular component organization or developmental processes, protein transport, immune system processes et al. Given that microglia influence sympathetic activation through cell-to-cell interactions, whether autocrine or paracrine, it is crucial to consider the potential connection between p300-mediated acetylation of histones and non-histone proteins within microglia at the regulatory site level. Eventually, we confirmed the top differential expressed protein-HMGB1 which enriched in protein transport process as the potential target. Interestingly, one of our previous studies conducted PVN targeting administration of anti-HMGB1 polyclonal antibody and attenuated central-cardiac sympathetic tone in rats after MI.[31] Whether p300 mediated sympathetic hyperactivation through lysine acetylation of HMGB1?

https://doi.org/10.2147/JIR.S524375

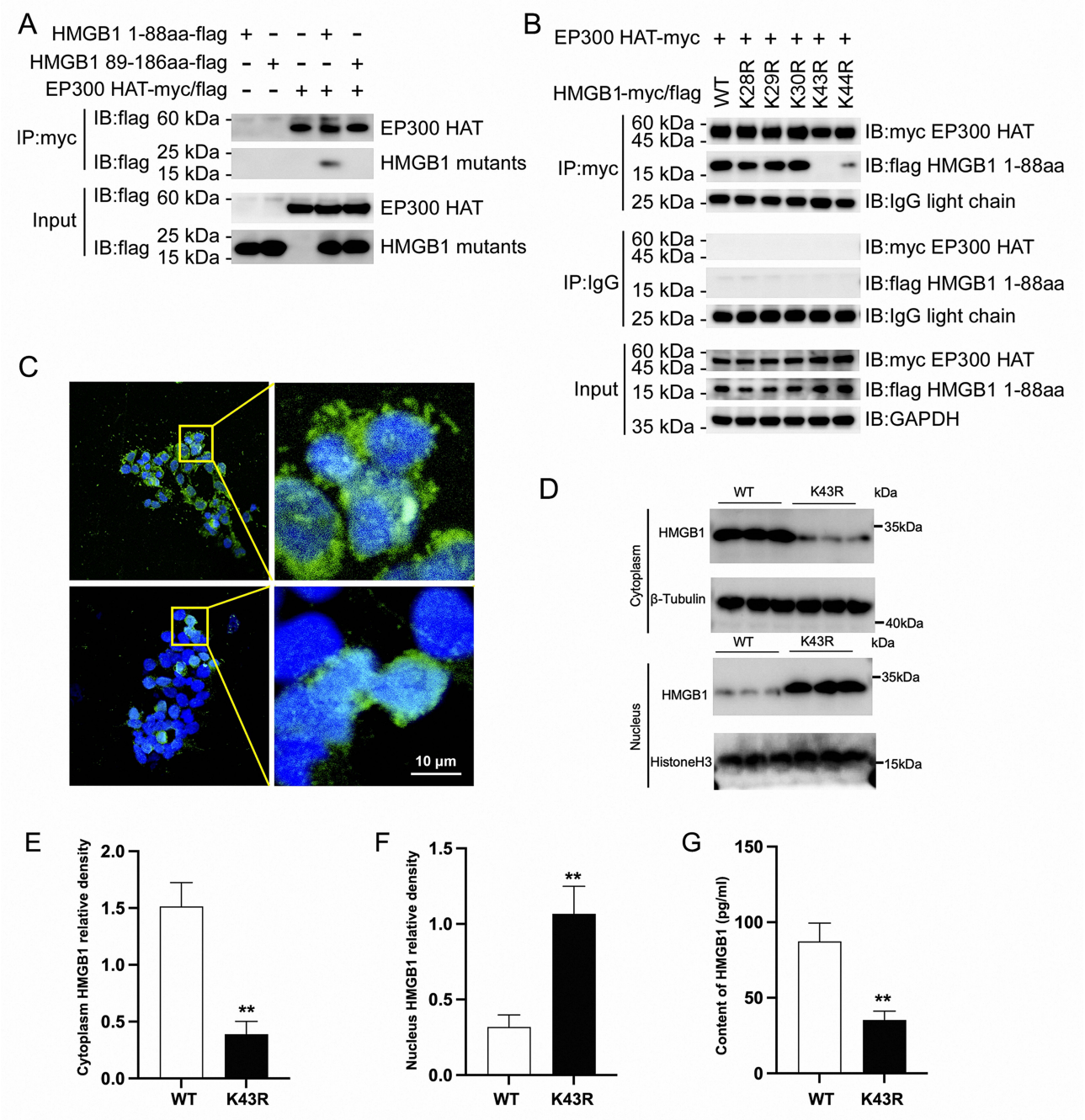

Figure 6 P300 acetylates HMGB1 at its K43 residue. (**A**) Co-transfection of Myc/Flag-tagged p300 into HEK293T cells with Flag-tagged HMGB1-A box or Flag-tagged HMGB1-B box. Immunoprecipitation was performed using an anti-Myc antibody, and Western blots were analyzed using the indicated antibodies. Cell lysates were immunoprecipitated with an anti-Myc antibody and subsequently analyzed using Western blotting. (**B**) Co-transfection of Myc-tagged p300 with HMGB1 truncation mutants or wild-type HMGB1 into HEK293T cells in the presence of HDAC inhibitors. Immunoprecipitation was performed using an anti-myc antibody and then analyzed using the specified antibodies. (**C**) Immunostaining for HMGB1 (green) and DAPI (blue) in the p300 /HMGB1 coinfection group (upper) and the p300/HMGB1 K43R mutant coinfection group (lower). Bar = 10 μm. (**D**) Representative Western blot illustrating cytoplasm/nucleus HMGB1 protein. (**E** and **F**) Qualification of cytoplasm and nucleus HMGB1 level, respectively. (**G**) ELISA for detecting HMGB1 content in cell culture supernatant in the p300 /HMGB1 coinfection group (upper panel) and p300/HMGB1 K43R mutant coinfection group. n = 4 per group. *T* test was applied for statistical analysis. $^{**}P < 0.01$ vs the WT group.
Abbreviations: ELISA, enzyme-linked immunosorbent assay; HMGB1, high-mobility group protein B1; WT, wild type.

HMGB1 is considered as an important endogenous peptides participating in microglia-mediated central neuroinflammation by actively secreted from activated immune cells and functions as a proclamatory cytokine,[32] acting as a mediator in the crosstalk between microglia/macrophages and neurons in an autocrine or paracrine manner.[33] The

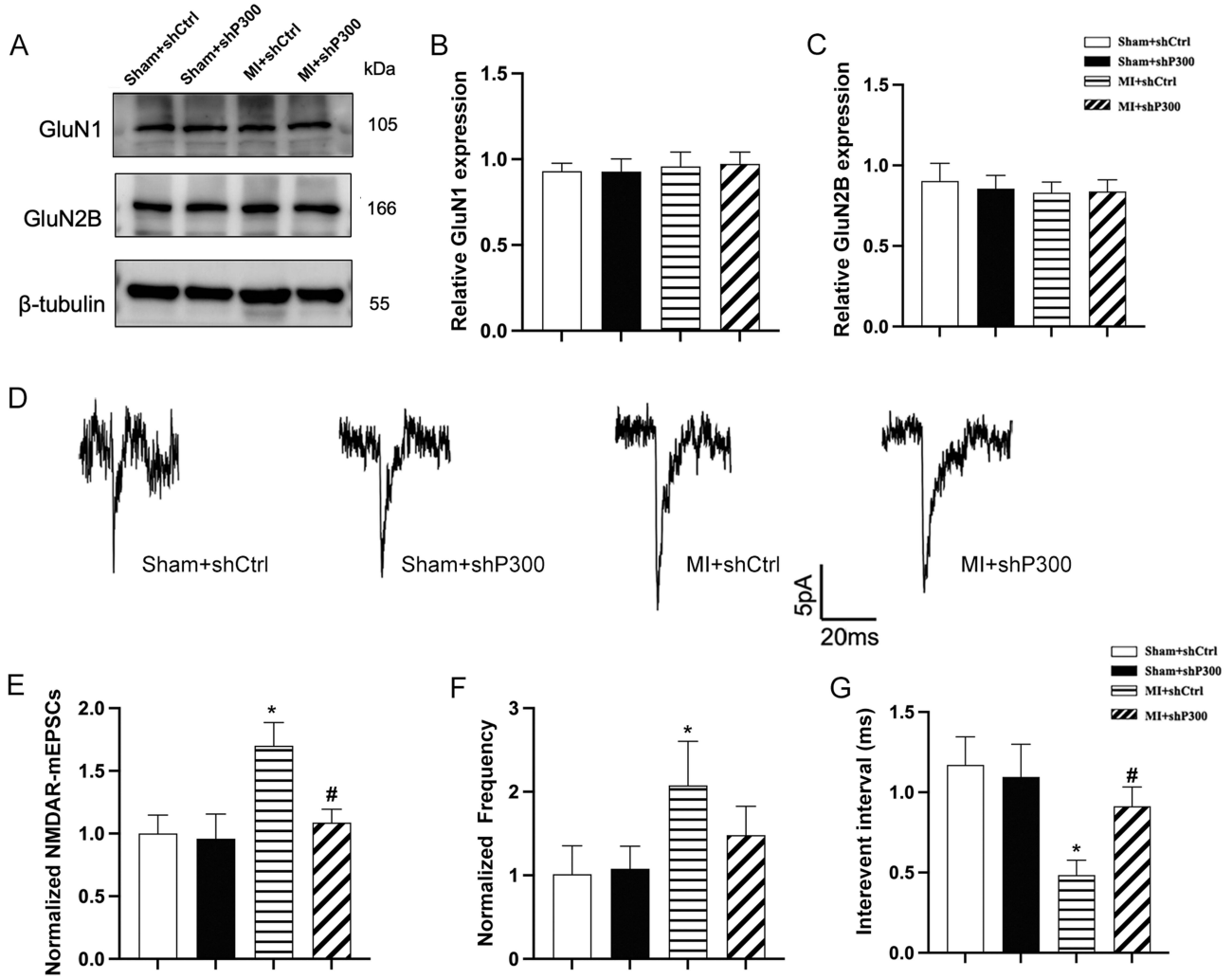

Figure 7 P300 knockdown diminished the increase in NMDA-mEPSCs post-MI. (**A**) Western blot showing the expression profiles of GluN1 (105kD) and GLuN2B (166kD) in PVN at day-7 post-MI. GluN1 and GluN2B expression were quantified relative to the β-tubulin (55 kD) levels. (**B** and **C**) Statistical bar graph of relative GluN1 and GLuN2B expression in Sham+shCtrl, Sham+shP300, MI+shCtrl, and MI+shP300 groups. (**D**) Representative single mEPSC currents of brain slices from Sham+shCtrl, Sham +shP300, MI+shCtrl, and MI+shP300 groups. (**E**) Statistical bar graph of normalized NMDAR-mEPSC current amplitude in the four groups. (**F** and **G**) Statistical bar graph of normalized NMDAR-mEPSC current frequency and interevent intervals in the four groups. n = 5 per group. *$P < 0.05$ vs the Sham+shCtrl group; # $P < 0.05$ vs the MI+shCtrl group.

mechanism of HMGB1 releasing into the extracellular space requires the transportation from the nucleus to cytoplasm. In macrophages, the equilibrium between acetylation and deacetylation of HMGB1 regulates the HMGB1 cytoplasm translocation. Nuclear transport of proteins larger than 45 kDa, such as HMGB1, requires NLS for nuclear import.[34] Reports on the primary deacetylated lysine sites of HMGB1 vary between K28, K30, K90, and K177. We found that the lysine acetylation site of HMGB1 by p300 is K43 evidenced by the fact that K43R mutation efficiently deacetylated HMGB1 and reversed its cytoplasm translocation. Consistently, in vivo study further showed that p300 silencing reversed HMGB1 acetylation and translocation. Next, we explored how this reversal occurred as it blocked the translocation process, which serves as a messenger mediating cell-to-cell contact between microglia and neurons. The downstream mechanism of this reversal remains unclear.

NMDARs and AMPARs in the hypothalamic PVN are critical in regulating sympathetic outflow.[35] We found no significant changes in expression of glutamate receptor. Whereas the increase of NMDAR-mEPSCs was observed as the mainly driver of sympathetic activation. Inhibition of p300 profoundly decreases NMDAR-mediated mEPSCs in PVN post-MI without affecting the expression of glutamate receptors. Therefore, we tested whether HMGB1 directly or indirectly facilitates NMDAR current. Through conducting molecular docking to estimate the likely combination of HMGB1 and glutamate NMDAR using Discovery

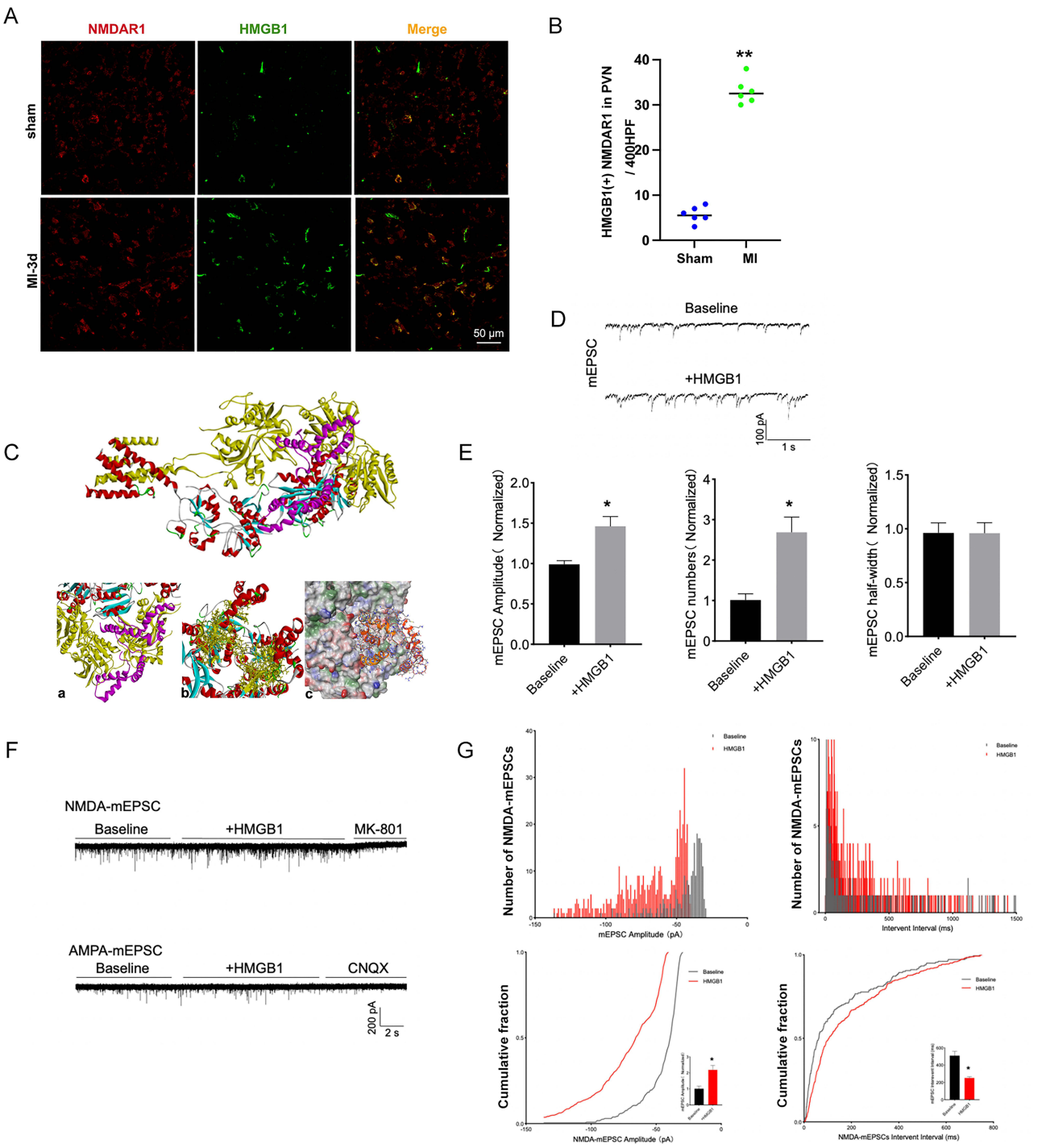

Figure 8 HMGB1 promotes NMDA-mEPSCs in PVN neurons. (**A**) Double-immunostaining for HMGB1 (green) and NMDAR1 (red) in the vehicle-MI group. (**B**) Quantification of HMGB1 positive NMDAR1 cells in the PVN. Bar = 50 μm. n = 6 per group. $^{**}P < 0.05$ vs sham group. (**C**) The structural diagram illustrates the optimal docking between the HMGB1 ligand (purple) and NMDAR receptor molecule (yellow band:GluN1, the other is GluN2B) is as follows: (a) The enlarged docking site of the optimal combination; (b) Receptor residues bound in the optimal structural diagram (overall, 43 amino acid residues); (c) Surface interaction in the optimal docking structure diagram, with blue representing positively charged surface areas, red indicating negatively charged surface areas, and green representing hydrophobic surface areas. (**D**) Recordings of representative spontaneous mEPSCs from PVN neurons before and after HMGB1 protein application via voltage-clamp in whole-cell recording mode, with a membrane potential held at −70 mV. (**E**) The statistical bar graph shows that HMGB1 significantly increased the amplitude and current numbers of mEPSCs without affecting the half-width of the mEPSCs in PVN neurons. (**F**) Representative NMDA-mEPSCs and AMPA-mEPSCs in response to HMGB1 and NMDA/AMPA antagonist MK-801 (10 μM)/CNQX (10 μM). (**G**) The upper panel shows the representative distribution of mEPSCs amplitude and frequency before (gray color) and after (red color) HMGB1 trigger. The lower panel shows the normalized cumulative distribution analysis of NMDA-mEPSCs amplitude and frequency in the same neurons as in (**D**), shows that HMGB1 induced a significant shift toward higher amplitude ($^{*}P < 0.05$) and decreased interevent interval (frequency) distribution ($^{*}P < 0.05$). HMGB1 did not affect AMPA-mEPSCs in PVN neurons. n = 5 per group. *T* test was applied for statistical analysis.

Abbreviations: AMPA, α-amino-3-hydroxy-5-methyl-4-isoxazolepropionic acid receptor-dependent; HMGB1, high-mobility group protein B1; mEPSCs, miniature excitatory postsynaptic currents; NMDAR, N-methyl-D-aspartate receptor; PVN, paraventricular nucleus; SD, standard deviation.

Studio software. We also found significant increase in co-staining of HMGB1 and NMDAR in PVN. Patch clamp study proofed he direct interaction of HMGB1 with NMDAR could further increase the NMDA current, thus facilitating postsynaptic sympathetic activation, which may explain the brain-cardiac axis of inflammation and sympathetic activation post-MI.

In addition, non-HMGB1 acetylation targets (eg, histones, transcription factors) that may also involved in p300-mediated modulation of sympathetic signaling. NF-κB, a key mediator of neuroimmune inflammatory responses, was identified as playing a pivotal role in both central and peripheral sympathetic excitation post-MI.[36] Specifically, p300 appears to be crucial in the regulation of NF-κB, either by interacting directly with NF-κB or by acetylation of H3K9 which facilitates NF-κB recruitment to the promoters of proinflammatory genes, such as IL-6, IL-8 and cyclooxygenase-2 (COX-2).[37] These alternative mechanisms will be further investigated in our future studies.

Clinical Implications

The epigenetics modification in the PVN evidenced for targeting central sympathetic activation in the treatment of ventricular arrhythmias refractory to conventional therapies. Sympathetic activity modification targeting PVN focusing on p300 blockage or HMGB1 translocation may hold promise for improving outcomes and reducing the risk of SCD in this patient population. The early discoveries could be expanded to application for sympathetic storm associated arrhythmia in clinical work.

Limitation

First, extrapolating data from rats rather than humans has potential limitations. For example, the AMI rat model differs from that of natural myocardial ischemia. Second, we did not investigate dominant-negative mutations in specific HMGB1 acetylation sites in vivo owing to technical limitations. Third, since microglia tended to resist AAV transduction, lack of viral efficiency and specificity to microglia in vivo was observed. In future study, we planned to improve transduction efficiency by AAV vectors driven under Iba promoter or capsid-modified AAV variants. Last but not the least, we did not investigate whether p300 knockdown affected other functions of p300 in the inflammatory reaction. Nonetheless, the outcomes of the current study provided therapeutic potential of central p300 signaling in confronting life-threatening ventricular arrhythmias following acute MI.

Conclusion

Our study suggested that p300-mediated translocation of HMGB1 may be a fundamental epigenetic mechanism in NMDAR-mediated central sympathetic activation post-MI. This finding provides new insights into neuroimmune cross-talk and brain-cardiac communication. Based on current findings, we aim to further develop site-specific deacetylation techniques for HMGB1, thus enabling precise control over sympathetic activation following MI.

Funding

National Natural Science Foundation of China (81900296, 82200362, 82300354, 32400994), the Higher Education Youth Innovation Team Plan of Shandong Province (2022KJ191), the Natural Science Foundation of Shandong Province (ZR2020MH024), the cultivation Fund for the First Affiliated Hospital of Shandong First Medical University (QYPY2021NSFC0613) and Shandong Provincial Key Discipline Construction Project of Traditional Chinese Medicine.

Disclosure

The authors report no conflicts of interest in this work.

References

1. Li T, Mu N, Yin Y, et al. Targeting AMP-activated protein kinase in aging-related cardiovascular diseases. *Aging Dis*. 2020;11(4):967–977. doi:10.14336/AD.2019.0901
2. Jiang S, Yang Y, Li T, et al. An overview of the mechanisms and novel roles of Nrf2 in cardiovascular diseases. *Expert Opin Ther Targets*. 2016;20 (12):1413–1424. doi:10.1080/14728222.2016.1250887

3. Yu JK, Liang JA, Franceschi WH, et al. Assessment of arrhythmia mechanism and burden of the infarcted ventricles following remuscularization with pluripotent stem cell-derived cardiomyocyte patches using patient-derived models. *Cardiovasc Res*. 2022;118(5):1247–1261. doi:10.1093/cvr/cvab140
4. Shi Y, Li Y, Yin J, et al. A novel sympathetic neuronal GABAergic signalling system regulates NE release to prevent ventricular arrhythmias after acute myocardial infarction. *Acta Physiologica*. 2019;227(2):e13315. doi:10.1111/apha.13315
5. Kluge N, Dacey M, Hadaya J, et al. Rapid measurement of cardiac neuropeptide dynamics by capacitive immunoprobe in the porcine heart. *Am J Physiol Heart Circulatory Physiol*. 2021;320(1):H66–h76. doi:10.1152/ajpheart.00674.2020
6. Yin J, Wang Y, Hu H, et al. P2X(7) receptor inhibition attenuated sympathetic nerve sprouting after myocardial infarction via the NLRP3/IL-1β pathway. *J Cell Mol Med*. 2017;21(11):2695–2710. doi:10.1111/jcmm.13185
7. Wang Y, Hu H, Yin J, et al. TLR4 participates in sympathetic hyperactivity Post-MI in the PVN by regulating NF-κB pathway and ROS production. *Redox Biol*. 2019;24:101186. doi:10.1016/j.redox.2019.101186
8. Sapp RM, Chesney CA, Springer CB, et al. Race-specific changes in endothelial inflammation and microRNA in response to an acute inflammatory stimulus. *Am J Physiol Heart Circ Physiol*. 2021;320(6):H2371–H2384. doi:10.1152/ajpheart.00991.2020
9. Yang M, Zhang Y, Ren J. Acetylation in cardiovascular diseases: molecular mechanisms and clinical implications. *Biochim Biophys Acta Mol Basis Dis*. 2020;1866(10):165836. doi:10.1016/j.bbadis.2020.165836
10. Mohanraj R, Hu H, Xuan Y, et al. Targeted NGF siRNA delivery attenuates sympathetic nerve sprouting and deteriorates cardiac dysfunction in rats with myocardial infarction. *PLoS One*. 2014;9(4):e95106.
11. Zhang Y, Cai Z, Shen Y, et al. Hydrogel-load exosomes derived from dendritic cells improve cardiac function via Treg cells and the polarization of macrophages following myocardial infarction. *J Nanobiotechnol*. 2021;19(1):271. doi:10.1186/s12951-021-01016-x
12. Geng Z, Ye C, Tong Y, et al. Exacerbated pressor and sympathoexcitatory effects of central Elabela in spontaneously hypertensive rats. *Am J Physiol Heart Circulatory Physiol*. 2020;318(1):H124–h134. doi:10.1152/ajpheart.00449.2019
13. Kim YG, Han S, Choi JI, et al. Impact of persistent left superior vena cava on radiofrequency catheter ablation in patients with atrial fibrillation. *Europace*. 2019;21(12):1824–1832. doi:10.1093/europace/euz254
14. Yin J, Hu H, Li X, et al. Inhibition of Notch signaling pathway attenuates sympathetic hyperinnervation together with the augmentation of M2 macrophages in rats post-myocardial infarction. *Am J Physiol Cell Physiol*. 2016;310(1):C41–C53. doi:10.1152/ajpcell.00163.2015
15. Venereau E, De Leo F, Mezzapelle R, et al. HMGB1 as biomarker and drug target. *Pharmacol Res*. 2016;111:534–544. doi:10.1016/j.phrs.2016.06.031
16. Lu B, Antoine DJ, Kwan K, et al. JAK/STAT1 signaling promotes HMGB1 hyperacetylation and nuclear translocation. *Proc Natl Acad Sci USA*. 2014;111(8):3068–3073. doi:10.1073/pnas.1316925111
17. Wang X, Yang Y, Ren D, et al. JQ1, a bromodomain inhibitor, suppresses Th17 effectors by blocking p300-mediated acetylation of RORγt. *Br J Pharmacol*. 2020;177(13):2959–2973. doi:10.1111/bph.15023
18. Kuwahara S, Arima H, Banno R, et al. Regulation of vasopressin gene expression by cAMP and glucocorticoids in parvocellular neurons of the paraventricular nucleus in rat hypothalamic organotypic cultures. *J Neurosci*. 2003;23(32):10231–10237. doi:10.1523/JNEUROSCI.23-32-10231.2003
19. Ramirez DMO, Crawford DC, Chanaday NL, et al. Loss of Doc2-dependent spontaneous neurotransmission augments glutamatergic synaptic strength. *J Neurosci*. 2017;37(26):6224–6230. doi:10.1523/JNEUROSCI.0418-17.2017
20. Bhar-Amato J, Davies W, Agarwal S. Ventricular arrhythmia after acute myocardial infarction: 'the perfect storm'. *Arrhythm Electrophysiol Rev*. 2017;6(3):134–139. doi:10.15420/aer.2017.24.1
21. Marinelli S, Basilico B, Marrone MC, et al. Microglia-neuron crosstalk: signaling mechanism and control of synaptic transmission. *Semin Cell Dev Biol*. 2019;94:138–151. doi:10.1016/j.semcdb.2019.05.017
22. Paudel YN, Angelopoulou E, Piperi C, et al. Impact of HMGB1, RAGE, and TLR4 in Alzheimer's disease (AD): from risk factors to therapeutic targeting. *Cells*. 2020;9(2):383. doi:10.3390/cells9020383
23. Zhang X, Lei B, Yuan Y, et al. Brain control of humoral immune responses amenable to behavioural modulation. *Nature*. 2020;581(7807):204–208. doi:10.1038/s41586-020-2235-7
24. Cryan JF, O'Riordan KJ, Cowan CSM, et al. The microbiota-gut-brain axis. *Physiol Rev*. 2019;99(4):1877–2013. doi:10.1152/physrev.00018.2018
25. Hu H, Wu H, Zhu T, et al. Long-term transcranial ultrasound stimulation regulates neuroinflammation to ameliorate post-myocardial infarction cardiac arrhythmia and remodeling. *Heart Rhythm*. 2024.
26. Chen J, Yin D, He X, et al. Modulation of activated astrocytes in the hypothalamus paraventricular nucleus to prevent ventricular arrhythmia complicating acute myocardial infarction. *Int J Cardiol*. 2020;308:33–41. doi:10.1016/j.ijcard.2020.01.035
27. Zhu Y, Wang K, Ma Z, et al. SIRT1 activation by butein attenuates sepsis-induced brain injury in mice subjected to cecal ligation and puncture via alleviating inflammatory and oxidative stress. *Toxicol Appl Pharmacol*. 2019;363:34–46. doi:10.1016/j.taap.2018.10.013
28. Placek K, Schultze JL, Aschenbrenner AC. Epigenetic reprogramming of immune cells in injury, repair, and resolution. *J Clin Invest*. 2019;129(8):2994–3005. doi:10.1172/JCI124619
29. Ding HH, Zhang SB, Lv YY, et al. TNF-alpha/STAT3 pathway epigenetically upregulates Nav1.6 expression in DRG and contributes to neuropathic pain induced by L5-VRT. *J Neuroinflammation*. 2019;16(1):29. doi:10.1186/s12974-019-1421-8
30. Whedon SD, Cole PA. KATs off: biomedical insights from lysine acetyltransferase inhibitors. *Curr Opin Chem Biol*. 2023;72:102255. doi:10.1016/j.cbpa.2022.102255
31. Li P, Jie Y, YuGen S, et al. High mobility group box-1 in hypothalamic paraventricular nuclei attenuates sympathetic tone in rats at post-myocardial infarction. *Cardiol J*. 2019;26(5):555–563. doi:10.5603/CJ.a2018.0117
32. Zhang S, Hu L, Jiang J, et al. HMGB1/RAGE axis mediates stress-induced RVLM neuroinflammation in mice via impairing mitophagy flux in microglia. *J Neuroinflammation*. 2020;17(1):15. doi:10.1186/s12974-019-1673-3
33. Sekiguchi F, Domoto R, Nakashima K, et al. Paclitaxel-induced HMGB1 release from macrophages and its implication for peripheral neuropathy in mice: evidence for a neuroimmune crosstalk. *Neuropharmacology*. 2018;141:201–213. doi:10.1016/j.neuropharm.2018.08.040
34. Wang M, Gauthier A, Daley L, et al. The role of HMGB1, a nuclear damage-associated molecular pattern molecule, in the pathogenesis of lung diseases. *Antioxid Redox Signaling*. 2019;31(13):954–993. doi:10.1089/ars.2019.7818

35. Li Y, Lu YX, Chi HL, et al. Chronic blockade of NMDAR Subunit 2A in the hypothalamic paraventricular nucleus alleviates hypertension through suppression of MEK/ERK/CREB pathway. *Am J Hypertens*. 2021;34(8):840–850. doi:10.1093/ajh/hpab047
36. Qi L, Wang Y, Hu H, et al. m6A methyltransferase METTL3 participated in sympathetic neural remodeling post-MI via the TRAF6/NF-?B pathway and ROS production. *J Mol Cell Cardiol*. 2022;170:87–99. doi:10.1016/j.yjmcc.2022.06.004
37. Di Pietrantonio N, Di Tomo P, Mandatori D, et al. Diabetes and its cardiovascular complications: potential role of the acetyltransferase p300. *Cells-Basel*. 2023;12(3):431.